ACS OMEGA

Open Access

http://pubs.acs.org/journal/acsodf

Article

Managing Oxidative Stress Using Vitamin C to Improve Biocompatibility of Polycaprolactone for Bone Regeneration *In Vitro*

Elaf Akram Abdulhameed, K.G. Aghila Rani, Fatima Mousa AlGhalban, Ensanya A. Abou Neel, Nadia Khalifa, Khalil Abdelrazek Khalil, Marzuki Omar,* and Ab Rani Samsudin*

Cite This: *ACS Omega* 2024, 9, 31776−31788

Read Online

ACCESS | Metrics & More | Article Recommendations | Supporting Information

ABSTRACT: Increased oxidative stress in bone cells is known to negatively alter favorable bone regeneration. This study aimed to develop a porous polycaprolactone (PCL) membrane incorporated with 25 wt % Vitamin C (PCL-Vit C) and compared it to the PCL membrane to control oxidative stress and enhance biomineralization *in vitro*. Both membranes were characterized using SEM-EDS, FTIR spectroscopy, and surface hydrophilicity. Vitamin C release was quantified colorimetrically. Assessments of the viability and attachment of human fetal osteoblast (hFOB 1.19) cells were carried out using XTT assay, SEM, and confocal microscopy, respectively. ROS generation and wound healing percentage were measured using flow cytometry and ImageJ software, respectively. Mineralization study using Alizarin Red in the presence or absence of osteogenic media was carried out to measure the calcium content. Alkaline phosphatase assay and gene expression of osteogenic markers (alkaline phosphatase (ALP), collagen Type I (Col1), runt-related transcription factor 2 (RUNX2), osteocalcin (OCN), and osteopontin (OPN)) were analyzed by real-time PCR. SEM images revealed smooth, fine, bead-free fibers in both membranes. The FTIR spectrum of pure vitamin C was replaced with peaks at 3436.05 and 2322.83 cm^{-1} in the PCL-Vit C membrane. Vitamin C release was detected at 15 min and 1 h. The PCL-Vit C membrane was hydrophilic, generated lower ROS, and showed significantly higher viability than the PCL membrane. Although both PCL and PCL-Vit C membranes showed similar cellular and cytoskeletal morphology, more cell clusters were evident in the PCL-Vit C membrane. Lower ROS level in the PCL-Vit C membrane displayed improved cell functionality as evidenced by enhanced cellular differentiation with more intense alizarin staining and higher calcium content, supported by upregulation of osteogenic markers ALP, Col1, and OPN even in the absence of osteogenic supplements. The presence of Vitamin C in the PCL-Vit C membrane may have mitigated oxidative stress in hFOB 1.19 cells, resulting in enhanced biomineralization facilitating bone regeneration.

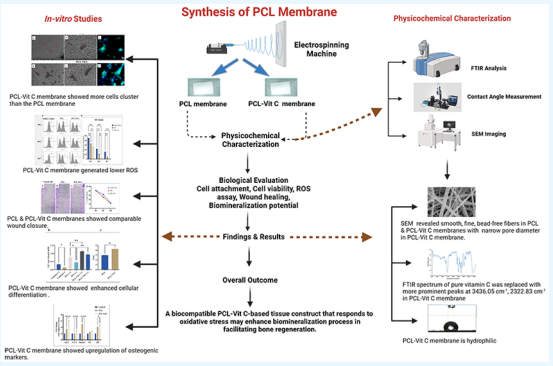

1. INTRODUCTION

Large bone defects are often encountered following trauma, surgical resections of skeletal tumors, or congenital anomaly. A biocompatible bone scaffold is needed to support the healing of these critical-size bone defects.[1] These bone defects are defined as those that will not heal spontaneously within a patient's lifetime.[2] Despite the expected characteristics of bone scaffolds used, including cyto-compatibility, immuno-compatibility, and biodegradability, the issue of biomaterial-generated oxidative stress in the implant microenvironment still poses a challenge that is poorly understood.[3] Moreover, several degradable biomaterials that are known to be "biocompatible" can induce significant oxidative stress and inflammation in the surrounding tissue during their degradation. Oxidative stress occurs when the production of reactive oxygen species (ROS), nitrogen species (RNS), and lipid peroxidation products surpasses the local antioxidant capacity of cells at the site of implantation.

Immunological evidence in wound healing studies indicates oxidative stress plays critical roles in dictating healing pathways toward inflammation, fibrosis, healing, or material rejection which are the major events that may occur during the implantation of biomaterials. Implanted materials stimulate oxidant formation, through the constant oxidative attack by immune cells and through their degradation products.[4] This may result in excessive or prolonged oxidant exposure, which can then lead to chronic inflammation and loss of the biomaterial's biocompatibility and function.[5] There is a need for a balanced expression of both oxidant production and elimination at the wound healing site for successful biomaterial

Received: March 25, 2024
Revised: May 31, 2024
Accepted: June 24, 2024
Published: July 12, 2024

implantation. Antioxidants delivered by injection or oral intake are usually not very effective due to rapid clearance, degradation, or low bioavailability at the biomaterial implantation site.[6] Therefore, frequent and high-dose administration is required, and consequently side-effects often arise. Alternatively, a functional antioxidative biomaterial scaffold that can sustainably and locally suppress oxidative stress may be designed for wound healing therapy and critical-sized bone defects. Designing biomaterials that modulate ROS and reactive nitrogen species (RNS) during the healing period is therefore a promising strategy to improve their outcomes *in vivo*.

Biomaterial design plays a major role in the generation of oxidants in tissues. The material properties that may induce and regulate oxidative stress include size and shape of the biomaterial, surface topography, wettability, mechanical properties, and material geometry.[7] However, the incorporation of an antioxidant into biomaterial would certainly be the prime strategy in mitigating oxidative stress at the local implantation site. This strategy includes the addition of antioxidant enzymes such as superoxide dismutase on to the surface of biomaterials, such as on polyethylene and polyurethane implants that resulted in a significant reduction of fibrotic encapsulation compared to nonmodified biomaterials.[8] Other investigators used metal chelators for polymers[9] and metal compounds[10] in metal-based biomaterials that are able to regulate levels of oxidative stress. Still some researchers used more complex techniques of incorporating substances that can modify the expression of gene coding for antioxidant proteins or ROS-producing enzymes within the healing implant environment.[11] However, the most common current approach in oxidative stress defense mechanism is embedding small antioxidant molecules such as vitamin C, vitamin E, curcumin, and Trolox into biomaterials.[3,12] Small antioxidant molecules are usually the preferred option because they are less specific than enzymes and they are less likely to lose their activity during incorporation in the biomaterial.[3] It is relatively easy to incorporate these small antioxidant molecules covalently or otherwise into polymers biomaterials for their release by diffusion and/or degradation. The choice of the polymer biomaterial and its final ability to perform an appropriate host response in a specific application is crucial to biomaterial-controlled antioxidant activity.

Polycaprolactone (PCL) is a biodegradable semicrystalline polymer which is widely used as bone tissue engineering scaffolds and delivery vehicles.[13] The properties of PCL, such as biocompatibility,[14] excellent mechanical properties, and economical production routes, make it an ideal choice for wound healing applications.[15] However, the hydrophobicity and slow biodegradation rate restrain its applications. Large numbers of techniques have been used to fabricate PCL micro/nanofibers, such as self-assembly phase separation, wet spinning, dry spinning, and electrospinning.[16] Among these, electrospinning has been widely used to fabricate nanofibers and is the most widely used approach to manufacture controllable highly porous fibrous membranes from certain viscosity of polymer fluids.[17] Several works incorporating antioxidants into PCL have been attempted with varying success.[18] The biocompatibility of the implant material may still be questionable if the oxidative stress element is not adequately addressed. Hence, the aim of this study was to develop a PCL membrane incorporated with Vit C (PCL-Vit C) to control oxidative stress and enhance bone mineralization *in vitro*.

2. MATERIALS AND METHODS

2.1. Preparation of Porous Electrospun Polycaprolactone Membrane with or without Vit C. Porous polycaprolactone membrane was synthesized using 11 wt % (80 000 MW, Sigma-Aldrich, St. louis. MO, USA) of PCL dissolved in a mixture of both chloroform (Sigma-Aldrich, St. Louis, MO, USA) and dimethyl sulfoxide (DMSO; Sigma-Aldrich, St. Louis, MO, USA) at a ratio of 9:1. First, the PCL was dissolved in a chloroform solution, and after complete dissolution, the DMSO was added to the dissolved PCL and stirred for 1 h at room temperature before electrospinning. The prepared mixture was then introduced into the electrospinning machine (Nanospinner, Inovenso, Istanbul, Turkey). The nanofibrous membrane was produced using a 21-gauge needle at a 22 cm needle-to-collector distance, a flow rate of 0.5 mL/h, and with a drum speed of 220 rotation per minute (RPM). The nanofibrous membrane was collected on the drum.[19] The temperature of the chamber in which the fibers were collected was 21−24 °C, and the humidity was 60−65%.[20]

For the Vitamin-C loaded PCL membrane (PCL-Vit C), the L-ascorbic acid (Bioworld, OH, USA) was used at 25 wt % in relation to the PCL.[21] The required amount of L-ascorbic acid (Bioworld, OH, USA) was dissolved in DMSO, then was added to the PCL dissolved in both chloroform and DMSO. Later, the nanofibrous membrane was drawn as explained above.

2.2. Membrane Morphology and Physicochemical Characterization. *2.2.1. Scanning Electron Microscopy with Energy-Dispersive X-ray Spectroscopy (SEM-EDS).* SEM-EDS was performed to conduct surface topography and elemental analysis. A square-shaped membrane of PCL and PCL-Vit C, measuring 1 × 1 cm, was employed for this purpose. The membranes were coated with gold using Quorum technologies SC7620, Tescan VEGA 3 XMU.[22] An Oxford Instruments X-max 50 EDS detector was employed to identify elements from three random regions across the membranes.

2.2.2. Fourier-Transform Infrared Spectroscopy (FTIR). Square-shaped (1 × 1 cm) samples of PCL and PCL-Vit C membranes were also used for FTIR. Jasco FTIR-6300 (Tokyo, Japan) was employed to obtain FTIR-ATR spectra of the PCL and PCL-Vit C membrane as well as the raw materials (pure PCL and Vit C powder). The spectra were recorded with a resolution of 2 cm^{-1} and 16 scans in the range region of 4000−400 cm^{-1} at room conditions at a constant temperature of 25 °C, which corresponds to the CH_2 group asymmetric and symmetric axial deformations (ν(C−H)).[23] Three samples were replicated for each sample type, and Origin Pro 8.5 software was used for data analysis. The attenuated total reflection (ATR) sampling mode was employed for spectra analysis, and baseline correction was performed.

2.2.3. Vitamin C Release. PCL-Vit C membranes incubated in 0.5 mL of PBS in a shaker incubator at 37 °C for 0 min, 15 min, 1 h, 6 h, 24 h, 48 h, up to day 7. The concentrations of ascorbic acid release from PCL-Vit C membrane were measured using an Ascorbic Acid Assay Kit (ab65656; Abcam, Cambridge, UK).

2.2.4. Contact Angle Measurement. Square-shaped (1 × 1 cm) samples were used. The water contact angle measurement

https://doi.org/10.1021/acsomega.4c02858
ACS Omega 2024, 9, 31776−31788

was conducted to evaluate the wettability and hydrophilicity of the PCL and PCL-Vit C membranes. A droplet of distilled water with a volume of 4 μL was placed on the surface of the membranes, and the sessile drop technique was performed using a Rame-hart automated goniometer (model 290-U1).[23] The mean contact angle value was determined by taking the average of three separate measurements at different time points: 0, 5, 15, and 35 min. The experiment was conducted in triplicate for a total number of three samples from each group.

3. BIOLOGICAL CHARACTERIZATION BY *IN VITRO* EXPERIMENTS

3.1. Cell Culture and Seeding. The human fetal osteoblast cells (hFOB 1.19) from Addexbio, USA were cultured in a medium consisting of Dulbecco's Modified Eagle Medium/Nutrient mixture F12 (DMEM/-F-12) supplemented with 10% fetal bovine serum (FBS) and 1% penicillin−streptomycin. The cells were maintained at a temperature of 37 °C in a humid atmosphere of 95% O_2 and 5% CO_2 throughout the experimental period. Upon reaching confluence, the cells were subcultured with 1x trypsin EDTA solution (59417 C; Sigma; USA), and the medium was replenished every 2 days. The PCL and PCL-Vit C membrane were prepared in a size of 1 × 1 cm, sterilized with UV for 30 min, and placed at the bottom of 12-well plates. Before seeding the cells, the membranes were incubated in 500 μL of complete culture media for 2 h in a CO_2 incubator. The media was aspirated out, and cells were seeded onto the membranes at a density of 1×10^5 cells per well in maximum volume of 50 μL and incubated at 37 °C with 5% CO_2 for another 2 h. The culture was replenished by adding an extra 1 mL of complete culture media and further incubated for downstream experiments.

3.2. Cell Attachment Studies by SEM and Confocal Microscopy. For SEM analysis, hFOB 1.19 cells were seeded onto the PCL and PCL-Vit C membranes and cultured for 7 days in a complete DMEM-F12 medium. Afterward, the cell-seeded membranes were washed in PBS, fixed in 2.5% glutaraldehyde for 1 h, and progressively dehydrated in ethanol. The cell seeded membranes were coated with gold using Quorum technologies SC7620 to prepare for SEM imaging using Tescan VEGA 3 XMU.[24]

For confocal microscopy, cell-seeded membranes were carefully washed three times with sterile PBS and then incubated with FITC-phalloidin (green) for detecting F-actin cytoskeleton, followed by DAPI for the nucleus (using a mounting medium containing DAPI; Abcam, USA) for 5 min. To observe the structure and function of the cytoskeleton after 7 days of cell seeding, the membranes were examined under a confocal microscope and images were captured (Nikon Eclipse Ti-S, Nikon Instruments Inc., USA). The fluorescence intensities of confocal microscopy images detailing cell attachment and spreading were calculated using ImageJ software (NIH, Bethesda, MD). The mean fluorescence intensity (MFI) was calculated from 5 randomly selected images acquired for each sample.

3.3. Cell Viability. The proliferation potential of hFOB cells grown on PCL and PCL-Vit C membranes was assessed using the XTT proliferation assay (Roche Diagnostics, Mannheim, Germany) through both direct and indirect methods. For the direct method, 5×10^4 cells were seeded onto the membranes and allowed to grow for 24−72 h in 24-well plates. The membranes were treated with the XTT reagent/activator mix and incubated for 4 h. 100 mL of extracts in duplicates from each well were collected, and absorbance at 450 nm was measured using the BioTek 800 TS microplate reader. The mean absorbance values were used to calculate the percentage cell viability. In the indirect method, extracts from PCL and PCL-Vit C membranes were prepared by incubating 1 × 1 cm size membranes in complete culture media for 24 h in a CO_2 incubator. The obtained extracts were directly added to hFOB 1.19 cells seeded on 96-well plates at a density of 5×10^3 cells per well and grown for a period of 24 h, 48 h, and 72 h. At the end of the incubation period, absorbance was measured using the same protocol as mentioned above.

3.4. ROS Detection and Measurement. ROS detection and measurement was done using cellular ROS assay kit (DCFDA/H2DCFDA - Cellular ROS Assay Kit, Abcam, UK). Briefly, the cells grown on PCL and PCL-Vit C membranes for 1, 2, and 7 days were harvested and incubated with the ROS assay reagent. Cells treated with H_2O_2 served as positive control in the experiment. 2 mL of the ROS assay reagent was added onto cells suspended in the ROS buffer and further incubated in a CO_2 incubator for 1 h. The cells were then analyzed by flow cytometry using FACS Aria III (Becton Dickinson, USA).[25]

3.5. Wound Healing Assay. A wound healing assay was performed using the PCL and PCL-Vit C membranes culture extracts as mentioned in the indirect method of cell viability. Cells grown in complete culture media were washed with PBS, followed by addition of media containing 2.5% FBS for 24 h. This method of serum starvation was performed to arrest the normal metabolic activities of the cells. The cells were seeded onto the assay well-plates following the manufacturer's instructions and incubated, followed by addition of the extracts of PCL and PCL-Vit C membranes. The culture inserts were aligned in 24-well plates to obtain a wound field in the same direction. The inserts were removed to create a 0.9 mm gap and stained using cell staining dye at 0 h, 6 h, and 24 h, and migration across the gap was monitored using the wound healing assay kit (ab242285; Abcam, USA) following the manufacturer's instructions with an inverted microscope. The percentage of residual wound gap following cell migration for the control and study groups was calculated using ImageJ software.[26] The experiment was performed in triplicate, and eight images from each study group were analyzed using ImageJ software to calculate the percentage wound gap.

3.6. Mineralization Study. *3.6.1. Alizarin Red Staining.* hFOB 1.19 cells were seeded at a density of 5×10^4 cells on PCL and PCL-Vit C membranes placed in 24-well plates. Cells were grown on the membranes in the presence or absence of osteogenic factors (10^{-8} M dexamethasone, 10 mM beta glycerophosphate) for 14 days. hFOB 1.19 cells seeded with and without osteogenic factors were used as controls. The cells were then evaluated for matrix mineralization, using Alizarin Red S staining to determine calcium deposition by the osteoblast cells. Briefly, on day 14, the cells and cell-seeded membranes were washed in PBS, fixed in 4% paraformaldehyde solution for 15 min at room temperature, and then stained with 40 mM Alizarin Red S solution for 20 min at room temperature with gentle rocking. After removing the Alizarin Red S solution, the samples were washed three times with deionized water and imaged using an inverted phase-contrast tissue culture microscope (Olympus, CKX 41, NY, USA).[24]

To quantify the calcium content, 10% acetic acid (v/v) was added to the Alizarin Red-stained cells grown on PCL and PCL-Vit C membranes and incubated at room temperature

https://doi.org/10.1021/acsomega.4c02858
ACS Omega 2024, 9, 31776−31788

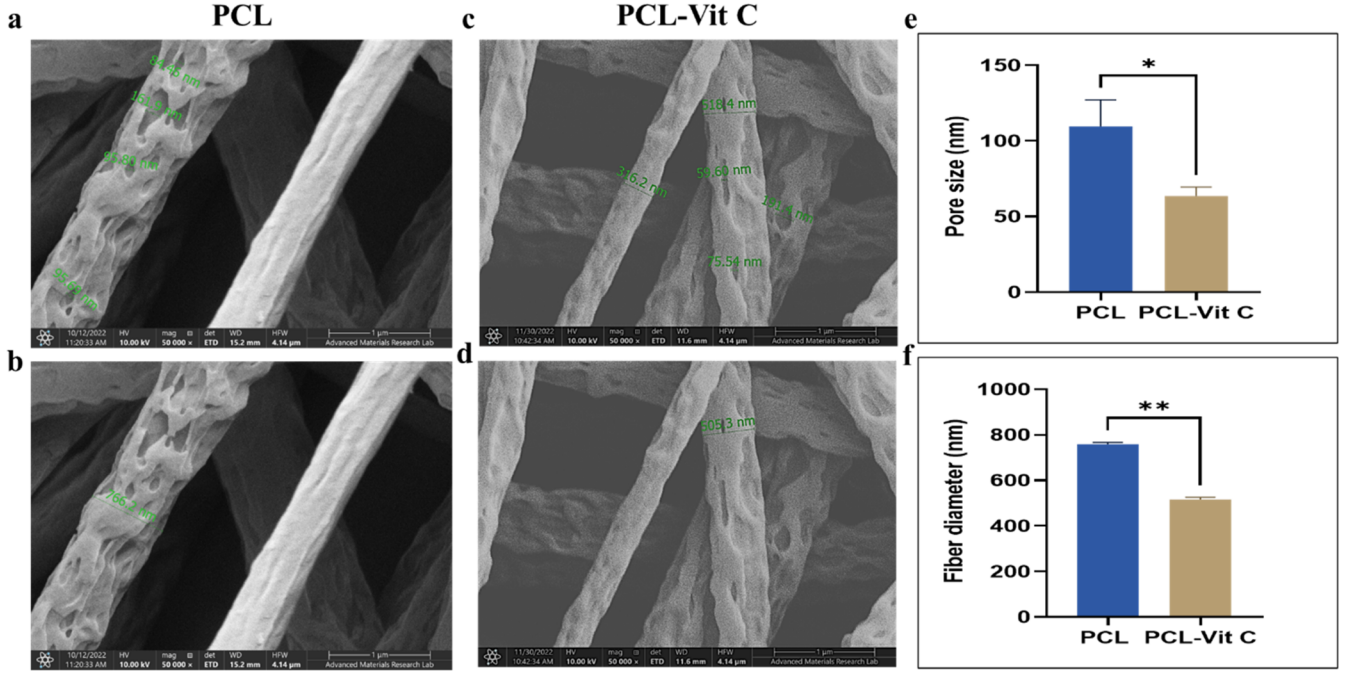

Figure 1. Morphology of PCL and PCL-Vit C membranes developed by electrospinning. SEM images revealed smooth, fine, bead-free structure in both PCL and PCL-Vit C membranes. SEM micrographs of (a) PCL membrane and (c) PCL-Vit C membranes showing irregularly shaped heterogeneous interconnected pores, with varying depth and wide size distribution. SEM micrographs of (b) PCL alone and (d) PCL-Vit C membranes showing varying fiber diameters. Bar graphs represent mean (e) pore size and (f) fiber diameter in PCL (n = 3) and PCL-Vit C membranes (n = 3). All data represent the mean ± SEM of three independent experiments. *p < 0.05; **p < 0.01 are indicated.

with gentle rocking for 30 min. The cells were then scraped out from the control culture wells, vortexed for 30 s, and incubated at 85 °C for 10 min, while the cell-seeded membranes were directly vortexed and incubated at the same temperature. Afterward, the samples were centrifuged for 15 min at 12,000 rpm, and the supernatant containing the cell lysates was collected for quantification using a plate reader at an absorbance of 405 nm. To quantify the total calcium release, a standard calibration curve for Alizarin dye was prepared.[24] All experiments were performed in triplicate for three independent samples.

3.6.2. Alkaline Phosphatase Activity Assay. Alkaline phosphatase (ALP) assay was performed using a colorimetric assay kit (ab83369; Abcam, USA) following the manufacturer's instructions.[24] Briefly, the cell lysates obtained from control cells and cells seeded on PCL and PCL-Vit C membranes in osteogenic conditions for 14 days were added to 96-well culture plates and incubated with pNPP solution for 60 min at room temperature. A STOP solution was then added to all the wells, and absorbance was measured at 405 nm. ALP standards were also prepared simultaneously following the kit instructions. All experiments were performed in triplicate for three independent samples.

3.7. Gene Expression of Osteogenic Markers by Real-Time RT PCR. To assess the osteogenic differentiation potential of hFOB 1.19 cells on PCL and PCL-Vit C membranes, the expression levels of mRNA for alkaline phosphatase (ALP), collagen Type I (Col 1), Runt-related transcription factor 2 (RUNX-2), osteocalcin (OC), and osteopontin (OP) were analyzed after a 14-day culture in osteogenic conditions. Total RNA was extracted from the cells harvested by trypsinization from both PCL and PCL-Vit C membranes using the RNeasy kit (Invitrogen, USA), and the RNA samples were evaluated for quality and concentration with the NanoDrop ND1000 (Thermo Fisher Scientific, USA). Subsequently, first-strand cDNA was synthesized using the HighScript cDNA synthesis kit (Thermo Fisher Scientific, USA), and the expression levels of osteogenic genes were determined using 5X FIREPOl SYBR Green Mix (Solisbiodyne). The reaction was conducted using gene-specific primer sequences, with glyceraldehyde-3-phosphate dehydrogenase (GAPDH) serving as the internal control for data normalization. hFOB 1.19 cells grown in the absence of osteogenic medium served as experimental controls. The qPCR amplification was carried out with an initial denaturation at 95 °C for 10 min, followed by 40 cycles at 95 °C for 30s, 60 °C for 1 min, and 72 °C for 1 min, using the StepOne Thermocycler (Applied Biosystems, USA). The results were quantified using the ΔΔCt relative quantification method. All experiments were performed in triplicate for three independent samples.

4. STATISTICAL ANALYSIS

Statistical analysis was carried out using GraphPad Prism software (version 9.1, USA). Data were expressed as mean ± SEM. A two-way analysis of variance (ANOVA) with multiple comparisons was performed to identify the differences between the study groups, and an unpaired t test was used whenever differences between two groups were studied. A p-value of p < 0.05 was statistically significant.

5. RESULTS

5.1. Membrane Morphology and Physicochemical Characterization. *5.1.1. Scanning Electron Microscopy.* The morphology and microstructure of the PCL and PCL-Vit C fibers along with their diameter distribution are presented in Figure 1. SEM images revealed that both the

https://doi.org/10.1021/acsomega.4c02858
ACS Omega 2024, 9, 31776−31788

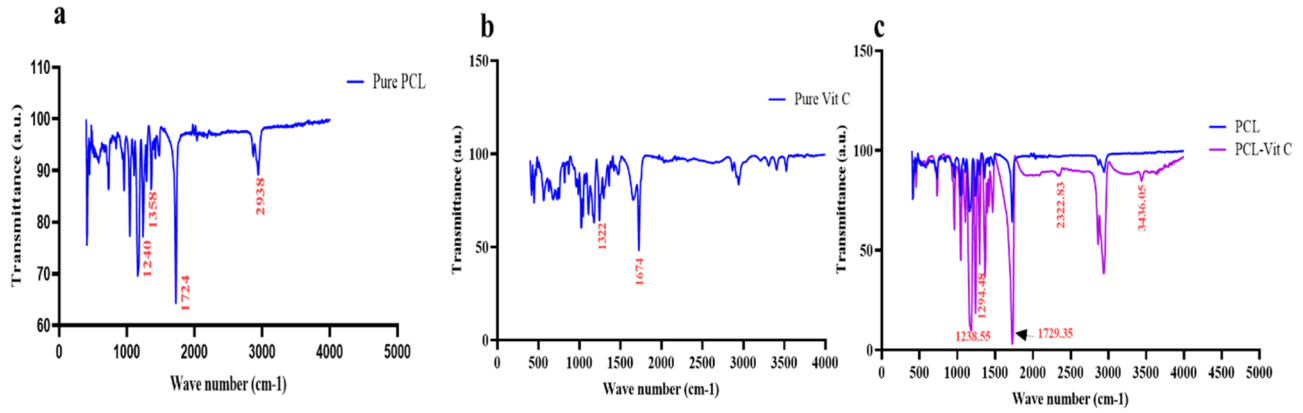

Figure 2. FTIR spectra of (a) pure PCL, (b) pure Vit C, and (c) PCL and PCL-Vit C membranes.

membranes exhibited a smooth, fine, bead-free, three-dimensional porous structure organized from heterogeneous interconnected pores. The nanofibers appeared nonwoven with random orientation from a structural point of view. Both PCL and PCL-Vit C membranes, however, showed variation in pore size and diameter (Figure 1a,b). In the PCL membrane, the mean diameter of pores is 109.46 ± 35.36 nm (Figure 1e) and the mean diameter of fibers produced is 759.05 ± 10.11 nm (Figure 1f); while in PCL-Vit C, the mean diameter of pores is 93.29 ± 58.16 nm and the mean diameter of fiber is 515.25 ± 14.07 nm. The pores for both membranes are irregularly shaped with varying depth and wide size distribution. The addition of 25 wt % Vitamin C significantly reduced both the pore size ($p < 0.05$) and fiber diameter ($p < 0.01$) of the PCL membrane (Figure 1e,f).

5.1.2. FTIR Spectroscopy. The FTIR spectrum of pure PCL is given in Figure 2a. The spectrum showed characteristic absorption bands at 2938 cm^{-1} (C−H), 1358 cm^{-1} (−CH_2 bending) vibration, asymmetric stretching vibration (C−O−C) at 1240 cm^{-1}, and carbonyl stretching vibration at 1724 cm^{-1}. The FTIR spectrum of pure Vit C (L-ascorbic acid) is represented in Figure 2b. The spectrum has stretching vibration of C−C double bond at 1674 cm^{-1} and enol hydroxyl at 1322 cm^{-1}. The peaks of pure Vit C were not observed in the FTIR spectra of the PCL-Vit C membrane; instead, the PCL-Vit C membrane showed more prominent peaks at 3436.05 and 2322.83 cm^{-1} which were not seen in the pure Vit C spectrum (Figure 2c). In addition, prominent peaks were observed at 1729.35 cm^{-1} (carbonyl stretching), 1294.48 cm^{-1} (C−O and C−C stretching), and 1238.55 cm^{-1} (asymmetric C−O−C stretching) in the PCL-Vit C membrane (Figure 2c).

The FTIR spectrum of PCL, PCL-Vit C membranes showed the common absorption bands at 2949 cm^{-1} (asymmetric −CH_2 stretching), 2868 cm^{-1} (symmetric −CH_2 stretching), 1726 cm^{-1} (carbonyl stretching), 1294 cm^{-1} (C−O and C−C stretching), 1239 cm^{-1} (asymmetric C−O−C stretching), and 1169 cm^{-1} (symmetric C−O−C stretching).

5.1.3. Vitamin C Release. A standard curve was generated according to the manufacturer's instructions using known concentrations of Vit C for quantifying the release of Vitamin C from PCL-Vit C membrane (Supplementary Figure 1a). We observed an initial burst release of Vitamin C from the PCL-Vit C membrane at 15 min of incubation in PBS. Subsequently, we noted a rise in Vitamin C levels at 1 h; however, following incubations beyond 1 h, we did not detect Vitamin C in the solution (Supplementary Figure 1b).

5.1.4. Contact Angle Measurement. The contact angle measurements of PCL and PCL-Vit C membranes are given in Table 1. The PCL Vit-C membrane was observed to be hydrophilic compared to PCL membrane. As time progressed, the contact angle of PCL-Vit C membrane was observed to be declining compared to PCL membrane. By 15 min of incubation, the contact angle of PCL-Vit C membrane reduced significantly ($p < 0.05$; 92.13° ± 0.53) compared to PCL membrane (126.66° ± 1.57). By 35 min, in the PCL-Vit C membrane, the contact angle was further reduced significantly ($p < 0.01$; 85.06° ± 0.73) while in the PCL membrane (119.10° ± 1.39), the contact angle was 119.10° at the same time point (Figure 3a,b). For a surface to be hydrophilic, the angle should be <90°; therefore, the PCL-Vit C membrane was found to be more hydrophilic than the PCL membrane.

Table 1. Contact Angle Measurement of the PCL and PCL-Vit C Membranes[a]

PCL		PCL-Vit C	
Time Point	Mean Angle	Time Point	Mean Angle
0 min	132.50° ± 0.61	0 min	126.01° ± 0.29
5 min	130.43° ± 0.74	5 min	121.36° ± 0.61
15 min	126.66° ± 1.57	15 min	92.13° ± 0.53*
35 min	119.10° ± 1.39	35 min	85.06° ± 0.73**

[a]The data is representative of three independent experiments ($n = 3$). *$p < 0.05$ and **$p < 0.01$ are indicated.

5.2. Biological Characterization of the PCL and PCL-Vit C Membranes *In Vitro*. *5.2.1. Cell Attachment and Spreading by SEM and Confocal Microscopy.* SEM and confocal microscopy images of cell-seeded PCL and PCL-Vit C membranes after 7 days of culture confirmed hFOB 1.19 cell attachment in both membranes (Figure 4). Clustered areas of cell attachment were more evident in PCL-Vit C membrane (Figure 4d−f) than in PCL membrane as confirmed by staining for the cytoskeletal marker, actin (Figure 4a−c). Cells were uniformly scattered, covering a larger area in PCL-Vit C membranes (Figure 4e) than in PCL membrane (Figure 4b). The cells seeded on PCL-Vit C membranes also displayed a multipolar polygonal shape with multiple long, tapering cytoplasmic processes/filapodial extensions, indicating a functionally active phenotype. In contrast, the cellular protrusions

https://doi.org/10.1021/acsomega.4c02858
ACS Omega 2024, 9, 31776−31788

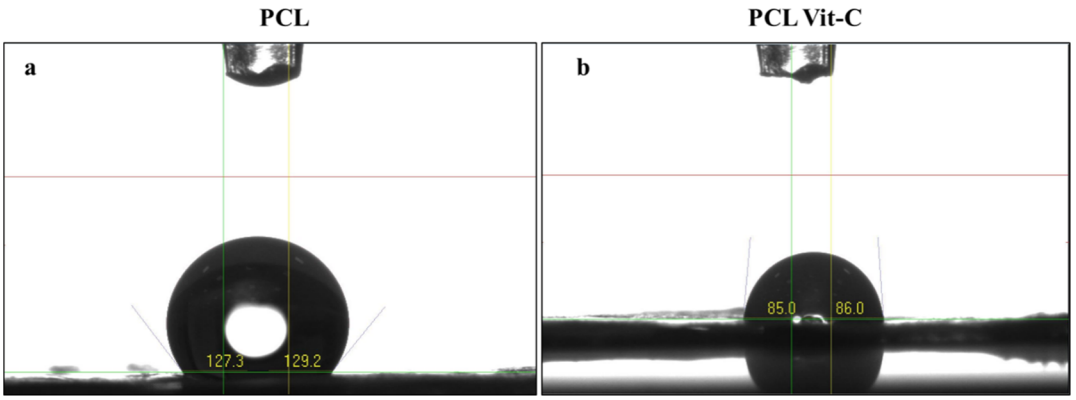

Figure 3. Contact angle images of a droplet of water on the surface of PCL and PCL-Vit C membranes. Representative images of contact angle measurements after exposing the surface of the (a) PCL and (b) PCL-Vit C membranes for 35 min are shown.

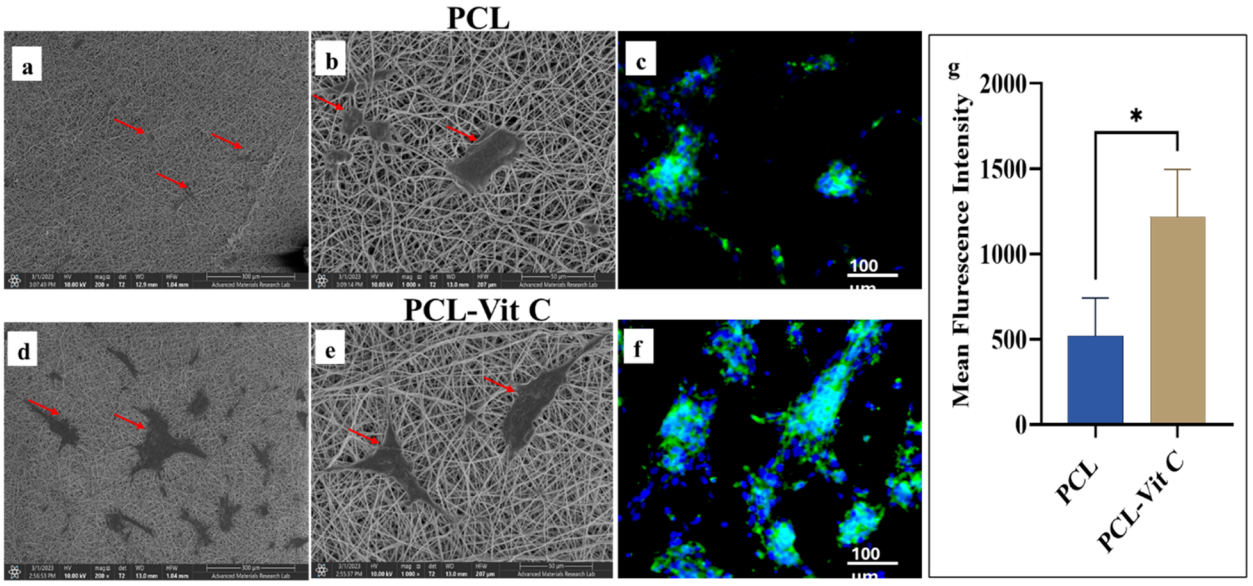

Figure 4. Cell attachment and spreading of hFOB 1.19 cells seeded onto the PCL and PCL-Vit C nanofibrous membranes. SEM analysis of hFOB 1.19 cells seeded on (a and b) PCL and (d and e) PCL-Vit C membranes. Cell attachment in (a and c) low magnification (scale bar = 300 μm) and (b and e) high magnification (scale bar = 50 μm) is shown. Confocal laser scanning micrographs of hFOB 1.19 cells seeded on (c) PCL and (f) PCL-Vit C nanofibrous membranes. Cells were stained with FITC-phalloidin (green) for F-actin cytoskeleton and DAPI for nucleus (blue). Cell clusters were more evident in PCL-Vit C membrane. Scale bar = 100 μm. (g) Mean fluorescence intensity (MFI) of hFOB 1.19 cells following adherence and spreading on PCL and PCL- Vit C membranes. * $p < 0.05$ is indicated.

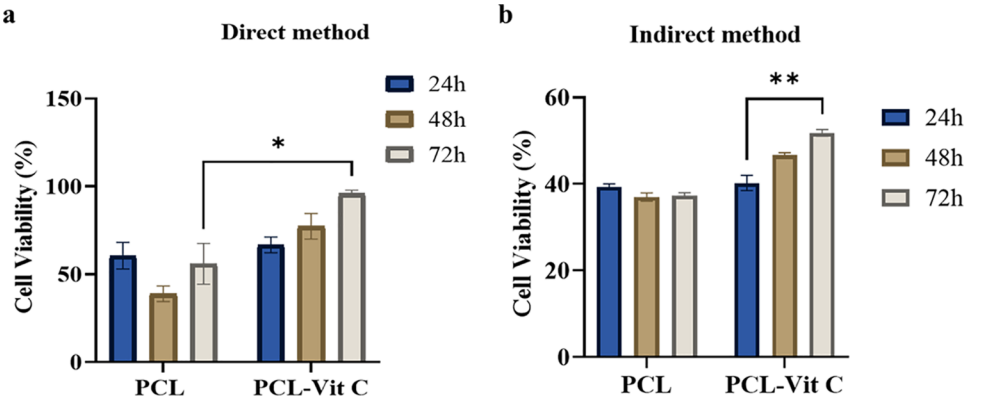

Figure 5. Cell viability by XTT assay after 24, 48 and 72 h of direct and indirect (extraction) culture of hFOB 1.19 cells on (a) PCL and (b) PCL-Vit C membranes. Bar graphs represent mean ± SEM percentage viability of cells. All data represent the mean ± SEM of three independent experiments. *$p < 0.05$ and **$p < 0.01$ are indicated.

https://doi.org/10.1021/acsomega.4c02858
ACS Omega 2024, 9, 31776−31788

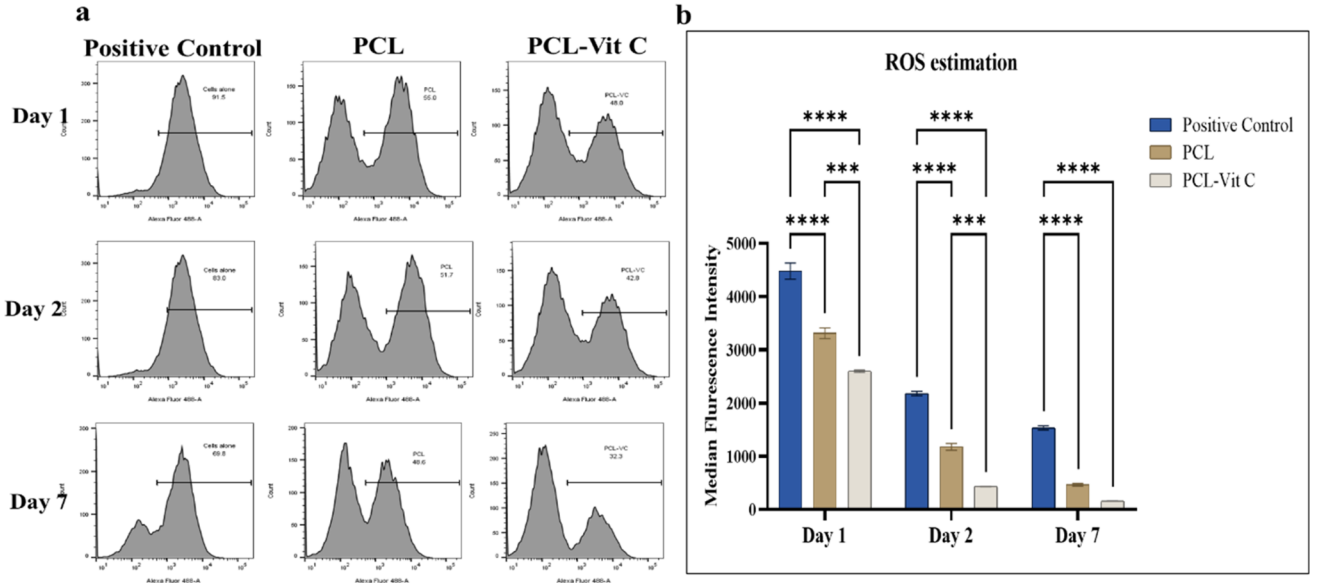

Figure 6. Flow cytometry analysis of ROS release in hFOB 1.19 cells grown on PCL and PCL-Vit C membranes at days 1, 2, and 7 in culture. (a) Representative flow cytometry histograms showing Alexa fluorophore 488 positive (right peak, ROS positive) and negative cells (left peak, ROS negative). (b) The histogram represents the mean fluorescent intensity (MFI) at indicated time points. All data represent the mean ± SEM of three independent experiments. ***$p < 0.001$, ****$p < 0.0001$ are indicated.

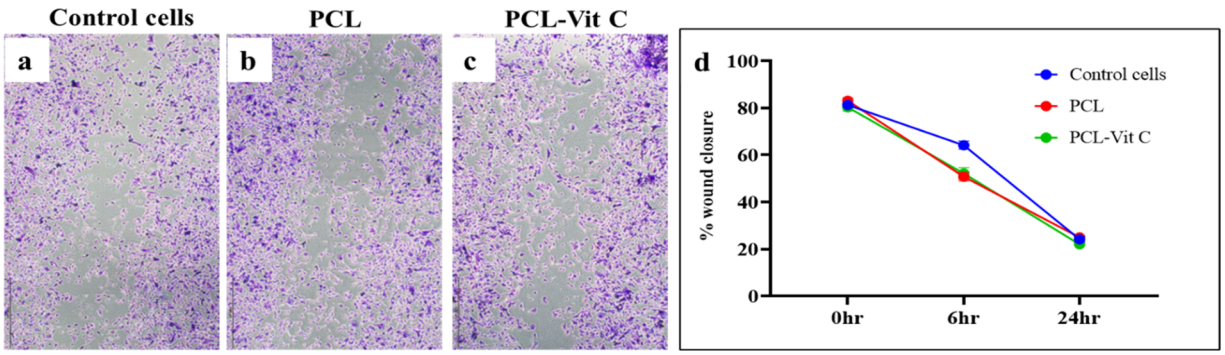

Figure 7. Wound healing assay. Representative images of wound scratch assay of hFOB 1.19 cells grown in (a) control 2.5% FBS containing culture medium, (b) extracts from PCL and (c) PCL-Vit C membranes at 24 h of culture. (d) Percentage (%) wound gap in the hFOB 1.19 cells treated with control 2.5% FBS containing culture medium, extracts from PCL, and PCL-Vit C membranes at 0, 6, and 24 h. All data represent the mean ± SEM of three independent experiments.

of hFOB 1.19 cells on the pure PCL membranes were poorly developed.

Confocal micrographs of the stained nuclei and actin cytoskeletons of hFOB 1.19 cells cultured on PCL and PCL-Vit C membranes further confirm the cell adhesion morphology of cells on both membranes. After 7 days of incubation, the actin cytoskeletons were well-developed in cells grown on PCL-Vit C (Figure 4c) compared with those on the PCL (Figure 4f) membranes. Cells in the PCL-Vit C membranes were able to penetrate to the interior deeper than the PCL membrane and the number of cells displaying green fluorescence for actin cytoskeleton attached to the PCL nanofiber in each plane was less compared with PCL-Vit C membrane. The presence of intact nanofibrils and porous microstructure in the PCL-Vit C membranes offered optimal cell attachment sites that favor the establishment of cell−matrix and cell−cell interactions through their extended filopodia. Quantification of mean fluorescence intensity (MFI) obtained from confocal microscopy images further confirmed that cellular attachment and spreading in the PCL-Vit C membrane was significantly ($p < 0.05$) higher than that in the PCL membrane (Figure 4g).

5.2.2. Viability Assay. XTT assay was performed to assess the cell viability at different time points by both direct and indirect (extraction method) as shown in Figure 5. The cells grown on the PCL-Vit C membranes exhibited significantly ($p < 0.05$) higher viability than the PCL membrane in the direct contact method (Figure 5b). The data demonstrate the efficacy of Vit C in promoting the attachment and proliferation of hFOB 1.19 cells. This finding aligns with the observations from SEM and confocal microscopy studies which show that the surfaces of PCL-Vit C membranes are evenly spread with hFOB 1.19 cells.

In contrast to the direct method, in the extraction method viability assay, there was no significant variation in cell viability among PCL and PCL-Vit C membranes (Figure 5a), suggesting that the extraction medium of both the membrane fibers had no cytotoxicity on meniscus of cells after culturing up to 72 h (Figure 5a). However, a significant increase in cell viability was observed at 72 h of culture in cells grown in PCL-

https://doi.org/10.1021/acsomega.4c02858
ACS Omega 2024, 9, 31776−31788

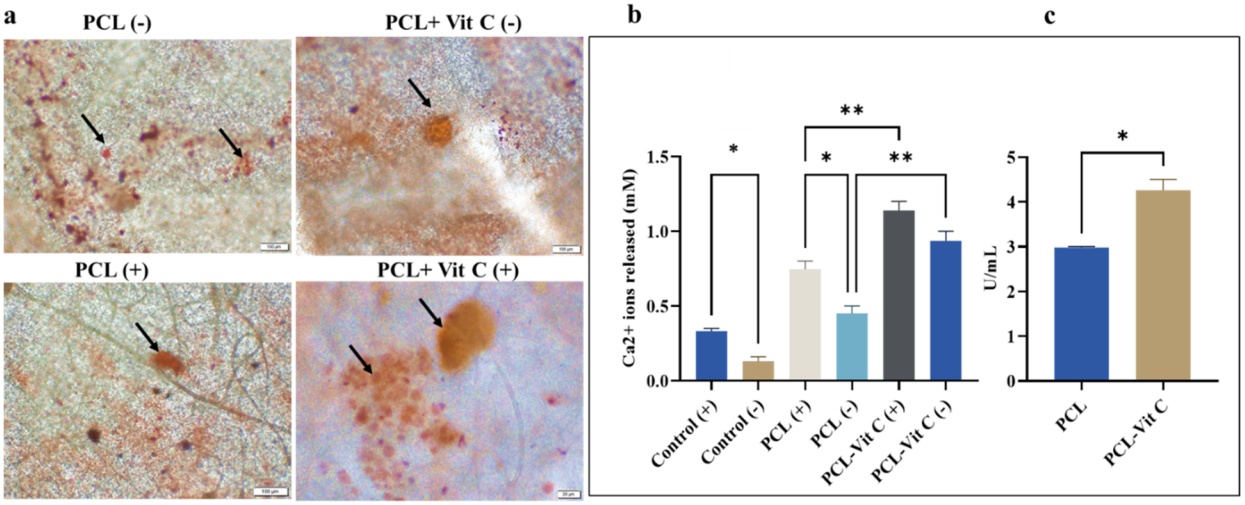

Figure 8. Extracellular matrix mineralization in hFOB cells grown in PCL and PCL-Vit-C membranes (a) Microscopic images showing calcification nodules (arrows) at day 14 in the presence (+) and absence (−) of osteogenesis supplements. Scale bar = 100 μm for all panels. (b) Quantification of alizarin Red S-stained mineralized nodules showing calcium release at day 14 in culture. (c) Quantification of alkaline phosphatase activity (ALP U/mL) at day 14 in culture. All data represent the mean ± SEM of three independent experiments. *$p < 0.05$, **$p < 0.01$ are indicated.

Vit C membrane extract compared to the PCL membrane at 24 h (Figure 5a; $p < 0.01$).

5.2.3. ROS Estimation. Cells grown on PCL membrane exhibited a highly significant decrease ($p < 0.0001$) in ROS generation at days 1, 2, and 7 of hFOB culture in comparison to the H_2O_2-treated positive controls (Figure 6). Similarly, cells grown on the PCL-Vit C membrane also exhibited a significant decrease in ROS generation at days 1 ($p < 0.001$), 2 ($p < 0.001$), and 7 ($p < 0.0001$) of hFOB culture in comparison to the H_2O_2 treated positive controls (Figure 5). PCL-Vit C membrane-grown cells showed a significant decline in ROS production at days 1 ($p < 0.001$) and 2 ($p < 0.001$) compared to PCL group. However, by day 7 the difference between the two membrane groups became negligible.

5.2.4. Wound Healing Assay. As shown in Figure 7, wound migration of the hFOB 1.19 monolayer cell culture showed a similar pattern among the control cells treated with 2.5% FBS-containing culture medium (Figure 7a), extracts from PCL (Figure 7b), and PCL-Vit C membranes (Figure 7c) at the 24 h time point. Figure 7d demonstrates a comparative graph of the effect of extracts from PCL and PCL-Vit C membranes on closing the wound gap at 0, 6, and 24 h. At 6 h, cells treated with PCL and PCL-Vit C membrane extracts achieved a wound closure of 50.79 ± 7.34% and 52.16 ± 10.27%, respectively. At the same time point, control cells achieved a wound closure of 60.55 ± 12.52%; nevertheless, the difference was not statistically significant ($p > 0.05$) in comparison to both the membrane groups. Likewise, at 24 h, the percentage wound closure among the control, PCL, and PCL-Vit C membrane extracts treated cells was reduced to 24.21 ± 5.31%, 28.46 ± 6.03%, and 22.01 ± 1.61%, respectively (Figure 7). Although a difference in percentage wound closure was observed in the PCL and PCL-Vit C membrane groups compared to control cells, the difference did not achieve statistical significance at any time points.

5.2.5. PCL-Vit C Membrane Enhanced Osteoblast Mineralization. Alizarin Red S staining displayed bright orange nodules in membranes supplemented with osteogenic media (+) compared to those without any supplements (−) (Figure 8a). A more intense staining was observed in the PCL-Vit C membrane on day 14 of culture than PCL at the same time point. It is important to note that PCL-Vit C membrane favored enhanced differentiation of hFOB cells compared to PCL membrane even in the absence of osteogenic supplements (Figure 8a). Quantification of Alizarin Red staining intensity further supported these observations. Significantly ($p < 0.001$) enhanced Ca^{2+} ions release was observed in PCL-Vit C membrane in the presence (+) and absence (−) of osteogenic supplements (Figure 8b).

Likewise, an enhanced ALP activity was observed in hFOB 1.19 cells grown in PCL-Vit C membranes by day 14 (Figure 8c). ALP activity of hFOB 1.19 cells seeded on the PCL-Vit C membrane was significantly higher ($p < 0.05$) compared to those on the PCL membrane (Figure 8c).

5.2.6. PCL Vit-C Enhanced Osteogenic Marker Expression. Expression of the osteogenic markers such as alkaline phosphatase (ALP), collagen type I (Col 1), runt-related transcription factor 2 (Runx2), osteopontin (OP), and osteocalcin (OC) in hFOB 1.19 cells cultured on the PCL membrane and PCL-Vit C membrane for 14 days were analyzed by quantitative real-time PCR (Figure 9). Expression of early osteogenic markers, ALP and Col 1, were significantly upregulated in hFOB 1.19 cells cultured on the PCL-Vit C membrane than in hFOB 1.19 cells grown on the PCL membrane ($p < 0.001$). It was also observed that the expression for the early osteogenic transcription marker Runx2 was higher in the PCL membrane compared to the PCL-Vit C membrane by day 14 (Figure 9). There was no significant difference in gene expression for OC among the two membranes. However, by day 14, cells grown on PCL-Vit C membrane exhibited a significantly upregulated expression for OP compared to those on the PCL membrane ($p < 0.05$; Figure 9).

6. DISCUSSION

Implantation of a biomaterial into host tissue will undoubtedly generate ROS that when produced in small amounts are essential for cellular physiological signal transduction processes while the condition becomes detrimental when the ROS level exceeds the local antioxidant capacity. Since Williams (2008)[1]

https://doi.org/10.1021/acsomega.4c02858
ACS Omega 2024, 9, 31776−31788

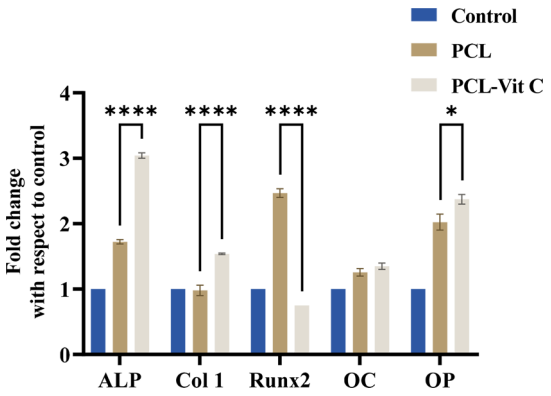

Figure 9. Realtime PCR analysis for expression of osteogenic markers in hFOB cells grown on PCL and PCL-Vit C membranes for 14 days. Histograms representing the relative changes (fold change) in the levels of expression of alkaline phosphatase (ALP), collagen type 1 (Col 1), Runt-related transcription factor 2 (Runx2), osteocalcin (OC), and osteopontin (OP) in hFOB cells. All results represent the mean ± SEM of three independent experiments. *$p < 0.05$ and ****$p < 0.001$ are indicated.

promoted the concepts of biocompatibility that dictate the mutually acceptable coexistence of biomaterials and tissues to perform a specific function without causing an unacceptable degree of harm to the host, a large number of strategies have been developed to mitigate uncontrolled inflammatory responses secondary to oxidative stress generated at the site of biomaterial implantation which may jeopardize the favorable healing pathway leading to failure.[1] Generally, endogenous ROS scavenging systems cannot protect the body against the effects of ROS overproduction. Traditional clinical therapy using systemic steroids or anti-inflammatory drugs is no doubt clinically effective but can cause side effects that affect multiple organs and threaten the general health of the host.[27] A more direct method of delivering antioxidants released from the biomaterial to the peri-implant microenvironment may be plausible, clinically safer, efficient, and more economical.[28]

In this study, the PCL-Vit C membrane seeded with hFOB 1.19 cells was designed as a tissue construct for bone tissue engineering with the main purpose of eliminating oxidative stress for enhancing biomineralization *in vitro*. Vit C was incorporated physically into the PCL membrane matrix. The synthesized PCL membrane showed porous nanofibrous morphology in the range of 109.46 ± 35.36 nm, which is favorable for osteoblast cell attachment. Incorporation of Vit C into the membrane matrix systems may allow easy release of the antioxidant to the cell culture environment via hydrolysis. SEM study showed the pores of PCL-Vit C membrane appeared obliterated with reduction in the diameter of fibers and this could be attributed to the increasing viscosity and decreasing conductivity of the spinning mixture with the addition of vitamin C. This finding agrees with a study done by Alipour et al. (2022)[23] who observed a reduction in the diameter of fibers from 1.24 ± 0.6 to 0.88 ± 0.4 μm with increasing incorporation of Vit C from 0 to 15 wt %.

The synthesized PCL and PCL-Vit C membranes in this study were validated using FTIR. The common peaks at 2938, 1358, 1240, and 1724 cm^{-1} in pure PCL are expected to match closely with the PCL membrane spectra, indicating the characteristic PCL structure is maintained. The PCL membrane may exhibit additional peaks or variations in peak intensity due to the membrane form or additives. The PCL-Vit C membrane lacks the distinct peaks of pure Vit C at 1674 and 1322 cm^{-1}, suggesting either interaction between PCL and Vit C components or masking of Vit C characteristic peaks by the dominant PCL structure or due to the low concentration of Vit C incorporated in the membrane. Another reason for the weak peak could also be due to the simultaneous alignment of the Vit C peak with the PCL peaks as mentioned in the study done by Alipour et al. (2022).[23] The presence of new peaks (3436.05 and 2322.83 cm^{-1}) or shifted peaks (e.g., 1729.35, 1294.48, and 1238.55 cm^{-1}) may suggest chemical interactions between PCL and Vit C, possibly through hydrogen bonding or other intermolecular forces, altering the chemical structure or conformation. On the other hand and based on previous literature,[29] the common peaks with high intensity in both PCL and PCL-Vit C membranes (e.g., carbonyl stretching at 1726 cm^{-1}) confirm the preservation of the PCL backbone structure.

The Vitamin C release studies performed in the current study showed an initial burst of Vitamin C from the PCL-Vit C membrane after 15 min and 1 h of incubation in PBS, followed by no further release. This pattern is in line with our expectations from the FTIR spectra of the PCL-Vit C membrane. The rapid initial release may have resulted from surface desorption or the presence of loosely bound vitamin C in PCL-Vit C membrane. We hypothesize that the stable integration of Vitamin C within the nanofibrous matrix is plausibly the cause for the absence of further release after 1 h.

While PCL membrane surfaces are generally hydrophobic, interestingly, incorporation of Vit C into the membrane reduced the water contact angle of the material and generated a more hydrophilic surface. This finding is in accordance with previous studies which have added Vit C into several types of scaffolds and confirmed the presence of the hydrophilic property of the biomaterial surface.[30] A hydrophilic surface encourages protein adsorption and cell adhesion at the cell–tissue interface, which is a critical immediate event in implantation of biomaterials.

The PCL membrane has been reported in many studies to produce a variable influence on the degree of ROS generation upon uptake by cells. Many workers claimed that PCL membrane surface topography, wettability, protein adsorption characteristics, and surface charges play an additional influence in ROS production.[31] In the present study, the exposure of hFOB 1.19 cells to PCL and PCL-Vit C membrane-induced stress is expected to generate intracellular ROS, which is crucial for normal cellular signaling and metabolism. However, the cells' inflammatory pathway may be stimulated when the level of ROS generation is overwhelmed and exceeds its physiological need. The results in this study showed a statistically significant rise in the level of ROS production in the PCL membrane in comparison to the PCL-Vit C membrane.

Our results suggest that incorporating Vit C into the PCL membrane can help mitigate ROS generation and maintain a more balanced redox environment within the cells. This reduction in ROS levels can contribute to improved cell survival and the overall success of tissue engineering strategies. These results agree with a study done by Ueno et al. (2011), who demonstrated oxidative stress induced by H_2O_2 significantly reduced the viability of osteoblast, its rate of proliferation, differentiation, and mineralization *in vitro*.[32] In a recent study by our group, AlHarthi et al. (2022) demonstrated that exposure of human osteoblast cells

https://doi.org/10.1021/acsomega.4c02858
ACS Omega 2024, 9, 31776−31788

(HOB) to titanium dioxide microparticles generated oxidative stress, which leads to release of proinflammatory cytokines MCP-1 and IL-8 which was measured after 24 h. The HOB cells were then treated with antioxidant Vit C and demonstrated a significant reduction in the generation of ROS and control of chemokines production in the HOB culture conditions.[33]

The biological evaluation of the PCL-Vit C membrane involved viability studies using hFOB 1.19 cells that demonstrated its superior biocompatibility compared to cells seeded on the PCL membrane, suggesting the influence of Vit C in eliminating oxidative stress generated by the biomaterial. The hFOB 1.19 cells on the PCL-Vit C membrane were morphologically healthy, showing good attachment and spread on the fibrillar membrane. Furthermore, comparison of the ROS assay between PCL membrane and PCL-Vit C showed a significantly lower generation of ROS in the PCL-Vit C group, which was even lower than the positive control by day 7.

It is known that cell culture incubated at ambient O_2 levels (95%) contribute to oxidative stress in both primary cells and immortalized cells.[34] In addition, the pro-oxidant nature of the cell culture medium and decreased availability of antioxidants, combined with higher-than-normal physiological oxygen tension would result in net increase in ROS in the hFOB 1.19 cell culture under the present experimental conditions. In fact, immortalized cells cultured under high oxygen tension might show higher inflammatory response and redox imbalance.[34] In this study, the addition of H_2O_2 has further simulated a higher oxidative stress condition in the hFOB 1.19 culture. The ability of PCL-Vit C in downregulating ROS suggests its efficiency in releasing and delivering antioxidants from the PCL matrix to the oxidants generated in the hFOB 1.19 cells in particular and to the cell culture medium environment in general.

Further evidence of PCL-Vit C enhancing cell growth capacity in this study was observed when the hFOB 1.19 cells were subjected to wound healing scratch assay. Our findings initially showed that at the 6 h period, there were minimal differences between the migratory rate of hFOB 1.19 in PCL and PCL-Vit C membranes compared to control cells, as demonstrated by the wide gap between the edges of the scratch wound margin in both test and control groups. However, by 24 h, the hFOB 1.19 cells at the wound edge in PCL-Vit C showed active polarization and migration into the wound space compared to the PCL membrane, demonstrating its two-dimensional cell migration ability in closing the gap. The presence of Vit C could have mitigated the generation of reactive oxygen species in the wound microenvironment secondary to scratch injury and triggered signaling pathways associated with cell proliferation and migration.[35]

The oxidative stress and endogenous antioxidant signaling pathways are still poorly understood. While vitamin C is a known potent antioxidant that is able to mitigate oxidative stress in cancer cells[36] and heavy metal exposure,[37] its antioxidative mechanisms in bone tissue is still controversial. However, a vitamin C-supplemented diet in Abalone has shown improvement in antioxidant capacity through Nrf2/Keap1 signaling.[38] Nuclear factor erythroid 2-related factor 2 (Nrf2) is a transcription factor expressed in many cell types, including osteoblasts, osteocytes, and osteoclasts. Nrf2 has been considered a master regulator of cytoprotective genes against oxidative stress, playing a key transcription role in regulating the expression of genes involved in the antioxidant and anti-inflammatory responses.[39] The key pathway of cellular resistance to oxidative stress was found to be Nrf2/Keap1 (kelch-like ECH-associated protein 1),[40] and many antioxidant enzymes regulated by the Nrf2/Keap1 pathway can remove reactive oxygen species, resists oxidative damage from the external environment and also enhances the endogenous antioxidant capacity of the body.[41] This pathway has shown significance in bone homeostasis, particularly in RANKL-induced osteoclastogenesis, where intracellular ROS levels are heightened. Previous studies showed potential effects of natural compounds such as 4-methylcatechol (4-MC), oroxylin A (OA), and notopterol (NOT) in regulating osteoclastogenesis and bone resorption by modulating oxidative stress and inflammation through Nrf2 activation.[42−44] Since Rana et al. reported that Nrf2-deficient osteoblasts also tend to lose their ability to differentiate and mineralize,[45] we hypothesize that Vitamin C incorporated PCL membranes may attenuate oxidative stress and inflammation via a similar ROS/Nrf2/Keap1 signaling axis in bone tissue.

Our current work demonstrates that both PCL and PCL-Vit C membranes can act as bone bioscaffolds to support the biomineralization process, with formation of calcium phosphate crystals within the extracellular matrix. Our results showed that the quantity of mineralization nodules in PCL-Vit C was higher than those in the PCL membrane even in the absence of osteogenic medium. Furthermore, besides addressing the free radicals produced by hFOB 1.19 cells, the PCL-Vit C membrane can provide a localized source of Vit C in the tissue culture condition, promoting collagen production and subsequent mineralization in accordance with previous studies by Hadzir et al. (2014).[35]

Our biomineralization results were further supported by quantitative real-time RT PCR analysis to identify the gene expression of osteogenic markers on day 14, such as alkaline phosphatase (ALP), osteocalcin (OCN), osteopontin (OPN), collagen type 1 (COL1), and RUNX2 in hFOB cells. High expressions of ALP and collagen type I were observed on day 14 in the PCL-Vit C group supporting extracellular matrix formation while OCN and OPN were equally expressed in both PCL-Vit C and PCL membrane-only, demonstrating mineralization activity in both groups. Expression of transcription factor RUNX2 was expectedly found to be low by day 14 in PCL-Vit C seeded osteoblast cells.

Although many authors have used other forms of antioxidants such as N-acetylcysteine, vitamin E, xanthan gum, and alginate,[46] Vit C has been selected in this study as the antioxidant molecule for direct ROS scavenging process due to its widely therapeutic use in chronic inflammatory diseases,[47] its long stay as a wound healing remedy,[48] and its recently identified role in mitigating the damaging inflammatory response in ischemia-reperfusion injury in bone.[49] Furthermore, Vit C can quickly diffuse into target cells and tissues to perform its therapeutic functions since it is smaller than other antioxidants.[50] Besides its antioxidant capacity, other favorable characteristics of the PCL membrane itself used in this study, including its numerous porosity, interconnectivity, and hydrophilic surface properties, could have contributed to the conducive biomimetic microenvironment for hFOB 1.19 cell growth, attachment, proliferation, differentiation, and mineralization of the extracellular matrix.

https://doi.org/10.1021/acsomega.4c02858
ACS Omega 2024, 9, 31776−31788

7. CONCLUSIONS

Managing wound healing approaches by incorporating drugs directly at implantation sites is one of the current strategies in regenerative medicine. This study has suggested the possibility of developing a biocompatible PCL-Vit C based tissue construct for bone tissue engineering that may respond to oxidative stress in the implantation microenvironment. Its antioxidative material property will prevent the propagation of uncontrolled inflammation and support the biomineralization process, facilitating tissue-material incorporation.

While oxidative stress inhibits osteoblastic differentiation and promotes apoptosis and the antioxidant Vit C activates osteoblastogenesis and inhibits osteoclastogenesis, there are still challenges ahead that are not well-understood. The concentration at which ROS is biologically relevant is yet to be deteremined, as is its association with the "biocompatibility" of PCL in performing a specific function. It is currently difficult to quantify and deliver antioxidant concentrations that are relevant and in particular that respond to variations of oxidative stress levels at the biomaterial implant site. The future may hold promise in developing ROS-scavenging bone scaffolds that help mitigate oxidative stress injury in the implantation cellular microenvironment and accelerate bone-tissue regeneration, expanding the horizon of biocompatibility of biomaterials.

■ ASSOCIATED CONTENT

Supporting Information

The Supporting Information is available free of charge at https://pubs.acs.org/doi/10.1021/acsomega.4c02858.

Supplementary Figure 1: a standard curve generated according to the manufacturer's instructions using known concentrations of Vit C for quantifying the release of Vitamin C from PCL-Vit C membrane; Vitamin C release from the PCL-Vit C membrane shown at 15 min and 1 h (PDF)

■ AUTHOR INFORMATION

Corresponding Authors

Marzuki Omar − *School of Dental Sciences, Universiti Sains Malaysia, Kubang Kerian, Kelantan 16150, Malaysia*; Email: marzukie@usm.my

Ab Rani Samsudin − *Oral & Craniofacial Health Sciences, College of Dental Medicine, University of Sharjah, Sharjah 27272, United Arab Emirates*; Email: drabrani@sharjah.ac.ae

Authors

Elaf Akram Abdulhameed − *Restorative & Preventive Dentistry Department, College of Dental Medicine, University of Sharjah, Sharjah 27272, United Arab Emirates; School of Dental Sciences, Universiti Sains Malaysia, Kubang Kerian, Kelantan 16150, Malaysia*

K.G. Aghila Rani − *Research Institute for Medical and Health Sciences RIMHS, University of Sharjah, Sharjah 27272, United Arab Emirates*; orcid.org/0000-0003-1962-5070

Fatima Mousa AlGhalban − *Research Institute for Medical and Health Sciences RIMHS, University of Sharjah, Sharjah 27272, United Arab Emirates*

Ensanya A. Abou Neel − *Restorative & Preventive Dentistry Department, College of Dental Medicine, University of Sharjah, Sharjah 27272, United Arab Emirates; UCL Eastman Dental Institute, Biomaterials & Tissue Engineering Division, Royal Free Hospital, London WC1E 6BT, U.K.*

Nadia Khalifa − *Restorative & Preventive Dentistry Department, College of Dental Medicine, University of Sharjah, Sharjah 27272, United Arab Emirates*

Khalil Abdelrazek Khalil − *College of Engineering, University of Sharjah, Sharjah 27272, United Arab Emirates*

Complete contact information is available at: https://pubs.acs.org/10.1021/acsomega.4c02858

Notes

The authors declare no competing financial interest.

■ ACKNOWLEDGMENTS

The authors thank Mr. Mohamed Shameer in the Advanced Materials Research Laboratory at the University of Sharjah for his contribution to the SEM-EDS, Ms. Fatima Mohamed Abla for her assistance in FTIR spectroscopy analyses, and Mr. Fahad Hassan for his assistance in contact angle measurements.

■ REFERENCES

(1) Williams, D. F. On the mechanisms of biocompatibility. *Biomaterials* **2008**, *29* (20), 2941−2953.

(2) Roddy, E.; DeBaun, M. R.; Daoud-Gray, A.; Yang, Y. P.; Gardner, M. J. Treatment of critical-sized bone defects: clinical and tissue engineering perspectives. *European Journal of Orthopaedic Surgery & Traumatology* **2018**, *28*, 351−362.

(3) Mouthuy, P.-A.; Snelling, S. J.; Dakin, S. G.; Milković, L.; Gašparović, A. Č.; Carr, A. J.; Žarković, N. Biocompatibility of implantable materials: an oxidative stress viewpoint. *Biomaterials* **2016**, *109*, 55−68.

(4) Chang, H.-H.; Guo, M.-K.; Kasten, F. H.; Chang, M.-C.; Huang, G.-F.; Wang, Y.-L.; Wang, R.-S.; Jeng, J.-H. Stimulation of glutathione depletion, ROS production and cell cycle arrest of dental pulp cells and gingival epithelial cells by HEMA. *Biomaterials* **2005**, *26* (7), 745−753.

(5) Lin, T.-h.; Tamaki, Y.; Pajarinen, J.; Waters, H. A.; Woo, D. K.; Yao, Z.; Goodman, S. B. Chronic inflammation in biomaterial-induced periprosthetic osteolysis: NF-κB as a therapeutic target. *Acta biomaterialia* **2014**, *10* (1), 1−10.

(6) Ghosal, K.; Taran Hazra, B.; Brata Bhowmik, B.; Thomas, S. Formulation development, physicochemical characterization and in vitro-in vivo drug release of vaginal films. *Current HIV research* **2016**, *14* (4), 295−306.

(7) Chu, C.-C.; von Fraunhofer, J. A.; Greisler, H. P. *Wound closure biomaterials and devices*; CRC Press, 2018.

(8) Udipi, K.; Ornberg, R. L.; Thurmond, K. B.; Settle, S. L.; Forster, D.; Riley, D. Modification of inflammatory response to implanted biomedical materials in vivo by surface bound superoxide dismutase mimics. *J. Biomed. Mater. Res.* **2000**, *51* (4), 549−560.

(9) van Lith, R.; Gregory, E. K.; Yang, J.; Kibbe, M. R.; Ameer, G. A. Engineering biodegradable polyester elastomers with antioxidant properties to attenuate oxidative stress in tissues. *Biomaterials* **2014**, *35* (28), 8113−8122.

(10) Fan, J.; Yin, J.-J.; Ning, B.; Wu, X.; Hu, Y.; Ferrari, M.; Anderson, G. J.; Wei, J.; Zhao, Y.; Nie, G. Direct evidence for catalase and peroxidase activities of ferritin−platinum nanoparticles. *Biomaterials* **2011**, *32* (6), 1611−1618.

(11) Gallorini, M.; Petzel, C.; Bolay, C.; Hiller, K.-A.; Cataldi, A.; Buchalla, W.; Krifka, S.; Schweikl, H. Activation of the Nrf2-regulated antioxidant cell response inhibits HEMA-induced oxidative stress and supports cell viability. *Biomaterials* **2015**, *56*, 114−128.

(12) (a) Gamna, F.; Spriano, S. Vitamin E: a review of its application and methods of detection when combined with implant biomaterials. *Materials* **2021**, *14* (13), 3691. (b) Anderson, J. M.; Rodriguez, A.;

Chang, D. T. Foreign body reaction to biomaterials. In *Seminars in immunology*; Elsevier, 2008; Vol. *20*, pp 86−100.
(13) Dash, T. K.; Konkimalla, V. B. Poly-ε-caprolactone based formulations for drug delivery and tissue engineering: A review. *J. Controlled Release* **2012**, *158* (1), 15−33.
(14) Fereshteh, Z.; Fathi, M.; Bagri, A.; Boccaccini, A. R. Preparation and characterization of aligned porous PCL/zein scaffolds as drug delivery systems via improved unidirectional freeze-drying method. *Materials Science and Engineering: C* **2016**, *68*, 613−622.
(15) Zhong, S.; Zhang, Y.; Lim, C. Tissue scaffolds for skin wound healing and dermal reconstruction. *Wiley Interdisciplinary Reviews: Nanomedicine and Nanobiotechnology* **2010**, *2* (5), 510−525.
(16) Agarwal, S.; Greiner, A.; Wendorff, J. H. Electrospinning of manmade and biopolymer nanofibers—progress in techniques, materials, and applications. *Adv. Funct. Mater.* **2009**, *19* (18), 2863−2879.
(17) Gautam, S.; Chou, C.-F.; Dinda, A. K.; Potdar, P. D.; Mishra, N. C. Surface modification of nanofibrous polycaprolactone/gelatin composite scaffold by collagen type I grafting for skin tissue engineering. *Materials Science and Engineering: C* **2014**, *34*, 402−409.
(18) (a) Wang, Y.; Wang, X.; Zhou, D.; Xia, X.; Zhou, H.; Wang, Y.; Ke, H. Preparation and Characterization of Polycaprolactone (PCL) Antimicrobial Wound Dressing Loaded with Pomegranate Peel Extract. *ACS omega* **2023**, *8* (23), 20323−20331. (b) Liang, R.; Zhao, J.; Li, B.; Cai, P.; Loh, X. J.; Xu, C.; Chen, P.; Kai, D.; Zheng, L. Implantable and degradable antioxidant poly (ε-caprolactone)-lignin nanofiber membrane for effective osteoarthritis treatment. *Biomaterials* **2020**, *230*, 119601.
(19) Sowmya, B.; Hemavathi, A.; Panda, P. Poly (ε-caprolactone)-based electrospun nano-featured substrate for tissue engineering applications: a review. *Progress in biomaterials* **2021**, *10* (2), 91−117.
(20) Vieira, T.; Rebelo, A. M.; Borges, J. P.; Henriques, C.; Silva, J. C. Electrospun Polycaprolactone Membranes Expanded with Chitosan Granules for Cell Infiltration. *Polymers* **2024**, *16* (4), 527.
(21) Agarwal, Y.; Rajinikanth, P.; Ranjan, S.; Tiwari, U.; Balasubramnaiam, J.; Pandey, P.; Arya, D. K.; Anand, S.; Deepak, P. Curcumin loaded polycaprolactone-/polyvinyl alcohol-silk fibroin based electrospun nanofibrous mat for rapid healing of diabetic wound: An in-vitro and in-vivo studies. *Int. J. Biol. Macromol.* **2021**, *176*, 376−386.
(22) Prasad, T.; Shabeena, E.; Vinod, D.; Kumary, T.; Anil Kumar, P. Characterization and in vitro evaluation of electrospun chitosan/polycaprolactone blend fibrous mat for skin tissue engineering. *J. Mater. Sci.: Mater. Med.* **2015**, *26*, 1−13.
(23) Alipour, H.; Saudi, A.; Mirazi, H.; Kazemi, M. H.; Alavi, O.; Zeraatpisheh, Z.; Abolhassani, S.; Rafienia, M. The effect of vitamin C-loaded electrospun polycaprolactone/poly (Glycerol Sebacate) fibers for peripheral nerve tissue engineering. *Journal of Polymers and the Environment* **2022**, *30* (11), 4763−4773.
(24) Al Qabbani, A.; Rani, K. A.; Syarif, J.; AlKawas, S.; Sheikh Abdul Hamid, S.; Samsudin, A.; Azlina, A. Evaluation of decellularization process for developing osteogenic bovine cancellous bone scaffolds in-vitro. *PLoS One* **2023**, *18* (4), No. e0283922.
(25) Aghila Rani, K.; Samsudin, A.; Abou Neel, E. A. Titanium dioxide doped phosphate glasses modulating pro-inflammatory macrophages reponses for tissue regeneration application. *Mater. Chem. Phys.* **2023**, *304*, No. 127857.
(26) Arab, A.; Aghila Rani, K.; Altell, R. T.; Ismail, A. A.; Alkawas, S.; Samsudin, A. The efficacy of salivary Histatin-1 protein in wound closure of nicotine treated human periodontal ligament fibroblast cells−In vitro study. *Archives of Oral Biology* **2022**, *141*, No. 105486.
(27) Panchal, N. K.; Sabina, E. P. Non-steroidal anti-inflammatory drugs (NSAIDs): A current insight into its molecular mechanism eliciting organ toxicities. *Food Chem. Toxicol.* **2023**, *172*, 113598.
(28) Liu, J.; Han, X.; Zhang, T.; Tian, K.; Li, Z.; Luo, F. Reactive oxygen species (ROS) scavenging biomaterials for anti-inflammatory diseases: From mechanism to therapy. *Journal of Hematology & Oncology* **2023**, *16* (1), 116.
(29) Azizi, M.; Azimzadeh, M.; Afzali, M.; Alafzadeh, M.; Mirhosseini, S. H. Characterization and optimization of using calendula offlcinalis extract in fabrication of polycaprolactone-gelatin electrospun nanofibers for wound dressing applications. *Journal of Advanced Materials and Processing* **2018**, *6* (2), 34−46.
(30) Janmohammadi, M.; Nourbakhsh, M. S.; Bonakdar, S. Electrospun skin tissue engineering scaffolds based on polycaprolactone/hyaluronic acid/l-ascorbic acid. *Fibers Polym.* **2021**, *22*, 19−29.
(31) Serrano, M. C.; Pagani, R.; Manzano, M.; Comas, J. V.; Portolés, M. T. Mitochondrial membrane potential and reactive oxygen species content of endothelial and smooth muscle cells cultured on poly (ε-caprolactone) films. *Biomaterials* **2006**, *27* (27), 4706−4714.
(32) Ueno, T.; Yamada, M.; Igarashi, Y.; Ogawa, T. N-acetyl cysteine protects osteoblastic function from oxidative stress. *J. Biomed. Mater. Res., Part A* **2011**, *99* (4), 523−531.
(33) AlHarthi, M. A.; Soumya, S.; Rani, A.; Kheder, W.; Samsudin, A. Impact of exposure of human osteoblast cells to titanium dioxide particles in-vitro. *Journal of Oral Biology and Craniofacial Research* **2022**, *12* (6), 760−764.
(34) Jagannathan, L.; Cuddapah, S.; Costa, M. Oxidative stress under ambient and physiological oxygen tension in tissue culture. *Current pharmacology reports* **2016**, *2*, 64−72.
(35) Hadzir, S. N.; Ibrahim, S. N.; Wahab, R. M. A.; Abidin, I. Z. Z.; Senafi, S.; Ariffin, Z. Z.; Razak, M. A.; Ariffin, S. H. Z. Ascorbic acid induces osteoblast differentiation of human suspension mononuclear cells. *Cytotherapy* **2014**, *16* (5), 674−682.
(36) Mostafavi-Pour, Z.; Ramezani, F.; Keshavarzi, F.; Samadi, N. The role of quercetin and vitamin C in Nrf2-dependent oxidative stress production in breast cancer cells. *Oncology letters* **2017**, *13* (3), 1965−1973.
(37) Li, Y.; Darwish, W. S.; Chen, Z.; Hui, T.; Wu, Y.; Hirotaka, S.; Chiba, H.; Hui, S.-P. Identification of lead-produced lipid hydroperoxides in human HepG2 cells and protection using rosmarinic and ascorbic acids with a reference to their regulatory roles on Nrf2-Keap1 antioxidant pathway. *Chemico-Biological Interactions* **2019**, *314*, No. 108847.
(38) Luo, K.; Li, X.; Wang, L.; Rao, W.; Wu, Y.; Liu, Y.; Pan, M.; Huang, D.; Zhang, W.; Mai, K. Ascorbic acid regulates the immunity, anti-oxidation and apoptosis in abalone Haliotis discus hannai Ino. *Antioxidants* **2021**, *10* (9), 1449.
(39) Sun, Y.-X.; Xu, A.-H.; Yang, Y.; Li, J. Role of Nrf2 in bone metabolism. *Journal of Biomedical Science* **2015**, *22*, 101.
(40) Sajadimajd, S.; Khazaei, M. Oxidative stress and cancer: the role of Nrf2. *Current cancer drug targets* **2018**, *18* (6), 538−557.
(41) Bartolini, D.; Dallaglio, K.; Torquato, P.; Piroddi, M.; Galli, F. Nrf2-p62 autophagy pathway and its response to oxidative stress in hepatocellular carcinoma. *Translational Research* **2018**, *193*, 54−71.
(42) Xu, Y.; Song, D.; Su, Y.; Chen, J.; Wu, L.; Lian, H.; Hai, N.; Jiang, J.; Zhao, J.; Xu, J. Pharmacology-based molecular docking of 4-methylcatechol and its role in RANKL-mediated ROS/Keap1/Nrf2 signalling axis and osteoclastogenesis. *Biomedicine & Pharmacotherapy* **2023**, *159*, No. 114101.
(43) Xian, Y.; Su, Y.; Liang, J.; Long, F.; Feng, X.; Xiao, Y.; Lian, H.; Xu, J.; Zhao, J.; Liu, Q. Oroxylin A reduces osteoclast formation and bone resorption via suppressing RANKL-induced ROS and NFATc1 activation. *Biochemical Pharmacology* **2021**, *193*, No. 114761.
(44) Chen, D.; Wang, Q.; Li, Y.; Sun, P.; Kuek, V.; Yuan, J.; Yang, J.; Wen, L.; Wang, H.; Xu, J.; et al. Notopterol attenuates estrogen deficiency-induced osteoporosis via repressing RANKL signaling and reactive oxygen species. *Frontiers in Pharmacology* **2021**, *12*, No. 664836.
(45) Rana, T.; Schultz, M.; Freeman, M. L.; Biswas, S. Loss of Nrf2 accelerates ionizing radiation-induced bone loss by upregulating RANKL. *Free Radic Biol. Med.* **2012**, *53* (12), 2298−2307.
(46) Chen, Q.; Shao, X.; Ling, P.; Liu, F.; Han, G.; Wang, F. Recent advances in polysaccharides for osteoarthritis therapy. *Eur. J. Med. Chem.* **2017**, *139*, 926−935.

https://doi.org/10.1021/acsomega.4c02858
ACS Omega 2024, 9, 31776−31788

(47) Ghalibaf, M. H. E.; Kianian, F.; Beigoli, S.; Behrouz, S.; Marefati, N.; Boskabady, M.; Boskabady, M. H. The effects of vitamin C on respiratory, allergic and immunological diseases: an experimental and clinical-based review. *Inflammopharmacology* **2023**, *31* (2), 653−672.
(48) Alyami, R.; Al Jasser, R.; Alshehri, F. A.; Alshibani, N.; Hamdan, S. B.; Alyami, R. A.; Niazy, A. A. Vitamin C influences antioxidative, anti-inflammatory and wound healing markers in smokers' gingival fibroblasts in vitro. *Saudi Dental Journal* **2023**, *35* (4), 337−344.
(49) Zhang, S.; Wotzkow, C.; Bongoni, A. K.; Shaw-Boden, J.; Siegrist, M.; Taddeo, A.; Blank, F.; Hofstetter, W.; Rieben, R. Role of the plasma cascade systems in ischemia/reperfusion injury of bone. *Bone* **2017**, *97*, 278−286.
(50) Kim, S.-A.; Jong, Y.-C.; Kang, M.-S.; Yu, C.-J. Antioxidation activity of molecular hydrogen via protoheme catalysis in vivo: an insight from ab initio calculations. *J. Mol. Model.* **2022**, *28* (10), 287.

https://doi.org/10.1021/acsomega.4c02858
ACS Omega 2024, 9, 31776−31788